


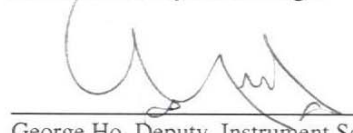
REV.	BY & DATE	DESCRIPTION	CHECK	APPROVED & DATE
Prepared by R.S., G.H., and C.S.	June 15, 2004	On-ground calibration report for the XRS instrument.		

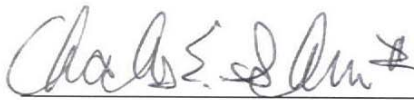
ADVISORY: This document has NOT been reviewed for export control and therefore may be subject to ITAR regulations or requirements.


 Ralph L. McNutt, Jr., Project Scientist and Cognizant Co-Investigator
 Date 6/18/04


 Robert Gold, Payload Manager
 Date 6/18/04


 Richard Starr, Instrument Scientist
 Date 6/22/2004


 George Ho, Deputy, Instrument Scientist
 Date 6/18/04


 Chuck Schlemm, Instrument Engineer
 Date 21 JUNE 2004

Released _____ Date _____

PART NUMBER	SIZE	NEXT ASSEMBLY	QTY./NA	USED ON	EFFECTIVITY - END ITEM SER. NO.	WEIGHT



THE JOHNS HOPKINS UNIVERSITY
APPLIED PHYSICS LABORATORY
 11100 JOHNS HOPKINS ROAD, LAUREL, MARYLAND 20723-6099

MESSENGER X-Ray Spectrometer (XRS) Calibration Report

FSCM NO.	SIZE	DRAWING NO.	REV.
88898	A	7388-9061	A
SCALE NONE	DO NOT SCALE PRINT		SHEET 1 OF 13

Table of Contents

INTRODUCTION	3
X-RAY REMOTE SENSING	3
INSTRUMENT DESCRIPTION	4
<i>Detectors</i>	4
<i>Collimator</i>	4
DETECTOR CALIBRATIONS	5
<i>Gas Proportional Counters</i>	5
<i>GPC Mapping</i>	5
<i>GPC Response and Efficiency</i>	6
<i>GPC Live Time</i>	7
<i>GPC Filter Thickness</i>	8
<i>Proton Charge Test</i>	8
<i>Collimator Field-of-View</i>	8
<i>Background Rejection</i>	9
Si-PIN SOLAR MONITOR	10
<i>Solar Monitor Response and Efficiency</i>	10
<i>Solar Monitor Live Time</i>	10
<i>Collimator Field-of-View</i>	11
REFERENCES	12

FSCM NO. 88898	SIZE A	DRAWING NO. 7388-9061	REV. A
SCALE	DO NOT SCALE PRINT		SHEET 2 of 13

INTRODUCTION

The Mercury Surface, Space Environment, Geochemistry, and Ranging mission (MESSENGER) will be launched in July 2004. MESSENGER will be the first spacecraft to visit Mercury since the Mariner 10 fly-bys of 1973 and 1974.

The X-Ray Spectrometer (XRS) is one of several instruments onboard the MESSENGER spacecraft that will study Mercury during one year of orbital operations beginning in 2011. The MESSENGER orbital period will be 12 hours and will be highly elliptical with periapsis ~200 km, and apoapsis ~15,200 km.

The XRS will measure characteristic X-ray emissions induced in the surface of the planet by the incident solar flux. The K-alpha lines for the elements Mg, Al, Si, S, Ca, Ti, and Fe will be detected with spatial resolution (at periapsis) on the order of 42 km when counting statistics are not a limiting factor. These measurements will be used to obtain quantitative information on elemental composition of Mercury's surface.

The X-ray spectrometer on the MESSENGER mission is a non-dispersive spectroscopic system. In this approach, the incoming X-ray photon is absorbed by the detector material and a signal proportional to the absorbed energy is measured by the detector as a voltage pulse at the detector output. An analog to digital conversion is then performed, and the count is binned by "pulse height" or energy loss and a spectrum is obtained. From an analysis of the pulse height spectrum, elemental composition can be inferred.

The choice among various types of X-ray detectors was strongly influenced by the constraints of the mission. For the MESSENGER mission, the detectors were chosen for the sensitivity in the energy regions of scientific interest, while also being consistent with the cost, mass, power and reliability constraints of the mission.

X-RAY REMOTE SENSING

The most prominent fluorescent lines for the major elements Mg, Al, Si, S, Ca, Ti, and Fe are the K-alpha lines (1-10 keV). The strength of these emissions from planetary surfaces is strongly dependent on the chemical composition of the surface as well as on the incident solar spectrum, but is of sufficient intensity to allow orbital measurement by detectors like those on the MESSENGER spacecraft.

In addition to line fluorescence, solar X-rays also can be coherently and incoherently scattered from a planetary surface, contributing an unwanted background signal. Astronomical X-ray sky sources, which could be sources of background, are eliminated at Mercury, because the XRS is collimated to a 12-degree field of view and the planet completely fills the field of view even at apoapsis so long as the instrument bore sight is near the planet's center.

The orbital portion of the MESSENGER mission, beginning in March 2011, will occur near an expected solar maximum. Greater solar activity will yield better statistics, shorter integration times, and hence higher resolution maps. The solar intensity decreases by three to four orders of magnitude from 1 to 10 keV. Fluorescent lines as well as the scatter-induced background, therefore, have greater intensity at

FSCM NO. 88898	SIZE A	DRAWING NO. 7388-9061	REV. A
SCALE	DO NOT SCALE PRINT		SHEET 3 of 13

lower energies. As the level of solar activity increases, relatively more output occurs at higher energies, the slope of the spectrum becomes less steep, and the overall magnitude of the X-ray flux increases. This process is called hardening. In general, only the lower energy X-ray lines from Mg, Al, and Si will be detected during quiet Sun periods. Fluorescence of the higher energy lines from S, Ca, Ti, and Fe will only be observed during flare activity. Solar output is highly variable, and can typically change by an order of magnitude or more within minutes. Because of its variability, the Sun's output must be monitored in order to be able to obtain quantitative results. An introduction to X-ray remote sensing techniques for geochemical analysis can be found in Yin *et al.* (1993).

INSTRUMENT DESCRIPTION

Detectors

The XRS consists of two separate detector units: the Mercury-pointing detectors and the solar monitor. The planetary-pointing detector package includes three large-area (10 cm² active area for each detector) sealed gas proportional counters (GPC) with thin (25 microns) Be windows. The large area provides the necessary sensitivity to achieve the desired spatial resolution and the Be windows absorb the lower energy X-rays (below 1 keV) which would otherwise dominate the detector count rate. The fill gas is P-10 (90% argon and 10% methane). The Be window is supported by a rectangular Be support structure. The detector housing is titanium with a graphite liner to absorb Ti line emission from the housing.

The sealed gas proportional counters chosen for this experiment are improved versions of instruments previously flown on Apollo 15 and 16 and the NEAR mission. The energy resolution of the gas proportional counters is not sufficient to resolve the low energy Mg, Al, and Si lines. As with the Apollo and NEAR missions it is necessary to use balanced filters to resolve these closely spaced lines (Adler *et al.* 1972 a, b, and c; Goldsten *et al.* 1997; Starr *et al.* 2000). Two of the detectors have thin absorption filters, approximately 6.7 microns thick, mounted externally. A Mg filter on one detector attenuates the Al and Si lines, and an Al filter on the other detector attenuates the Si line. The very steep absorption edges of the filters make the separation of the lower energy lines possible. The third detector has no filter. The energy resolution of these detectors is about 14% at 5.9 keV.

The sunward-pointing X-ray detector is a small Si-PIN photodiode, positioned on the spacecraft sun shield. The solar monitor experiences very strong X-ray emissions directly from the sun, especially during solar flares, so the active area of the solar monitor is only 0.0314 mm². A 76 micron thick Be window rejects the intense solar flux below 1 keV. The Si-PIN solar monitor achieves an energy resolution of ~600 eV at 5.9 keV.

During each integration period the XRS collects four 256-channel pulse height spectra: one for each of the three Mercury pointing detectors and one from the solar monitor.

Collimator

A collimator is used to restrict the X-ray spectrometer field of view to about 12 degrees. At periapsis (~200 km) this results in a spatial resolution of about 42 km. The collimator is also useful in reducing the cosmic X-ray background. The collimator uses a honeycomb design made of copper with 3% Be.

FSCM NO. 88898	SIZE A	DRAWING NO. 7388-9061	REV. A
SCALE	DO NOT SCALE PRINT		SHEET 4 of 13

The K, L and M X-ray lines excited in the collimator by solar X-rays, cosmic rays and planetary X-rays do not interfere with the surface line emissions.

DETECTOR CALIBRATIONS

In order to interpret the data collected by the XRS, a detailed understanding of the detector response is necessary. Efficiency and energy resolution as a function of energy, angular response, filter transmission as a function of energy, anti-coincidence efficiency, and rise-time rejection efficiency are most important.

Gas Proportional Counters

One advantage of using an older, but well known detector technology is that the characteristics of the system have been extensively studied and are well understood. The efficiency and resolution of gas proportional counters like those on MESSENGER have been measured many times. A detailed description of the response of proportional counters can be found in Knoll (1989).

The gas proportional counters (GPC) on MESSENGER have a chamber diameter of 40 mm and are filled with P-10 gas, a mixture of 90% argon and 10% methane, to an absolute pressure of 1500 mbar. The anode wire is gold-plated tungsten and has a diameter of 13 micrometers. In addition to the center wire, 14 anti-coincidence wires parallel to the anode wire are located near the Ti detector housing, outside of the graphite liner.

GPC Mapping

Uniformity of response over the 10 cm² active area of a GPC is important. Non-uniform electrical fields within the detector can cause detector efficiency to drop off near the edges of the window. Too great a drop off will result in an overall loss of efficiency. The rectangular Be support structure for the Be window of a GPC divides the 10 cm² active area into 15 smaller rectangles or cells. Our design goal was for cell efficiencies to be the same to within 10% for each GPC.

Cell Number

1	2	3	4	5
6	7	8	9	10
11	12	13	14	15

GPC01

82%	93%	94%	93%	90%
89%	99%	99%	100%	100%
74%	83%	86%	84%	84%

GPC02

82%	89%	89%	93%	86%
92%	100%	98%	95%	95%
77%	84%	85%	85%	81%

FSCM NO. 88898	SIZE A	DRAWING NO. 7388-9061	REV. A
SCALE	DO NOT SCALE PRINT		SHEET 5 of 13

GPC03

84%	93%	93%	93%	92%
91%	97%	100%	97%	93%
75%	82%	83%	82%	79%

GPC04

84%	90%	90%	90%	88%
94%	100%	98%	99%	97%
80%	88%	87%	87%	84%

It is apparent that there is a drop off in relative efficiency as you move further from the center cells. Combining the effect over all 15 cells gives a relative efficiency of 90%. There are two likely causes of this drop off in efficiency. The first is that closer to the edges (cells 1-5 and 11-15) the interaction path length is shorter. This increases the likelihood of escape events. The second possibility is a non-uniform electric field in the counters. This is also to be expected at some level. Monte Carlo modeling of the MESSENGER gas proportional counters yields an absolute efficiency of 89% at 5.9 keV when only the center cell (number 8) is irradiated. No drop off in efficiency is found for any of the cells in the center row (6-10). However, the efficiency of the side cells drops to ~86%, which corresponds to a relative efficiency compared to the center cell of 97%. This suggests most of the fall off in efficiency at the edges is due to poorer charge collection efficiency further from the center anode wire. While we do not meet our design goal of uniformity to 10% for all 15 cells in any of the tubes it should be understood that this was a goal and not a requirement for the proportional counters. The overall impact on the measurements to be made at Mercury is small and the science requirements of the XRS are still met.

GPC Response and Efficiency

Figure 1 displays the detector efficiency versus energy calculated for the MESSENGER gas proportional counters. A factor of 0.9 has been applied to the modeled efficiencies to correct for non-uniform field effects as explained in the previous section. The sharp features in the response of the Mg and Al-filtered detectors at 1.30 and 1.56 keV, respectively, are the filter K-edges. The very sharp feature seen in all three detectors at 3.20 keV is the K- edge in argon, the primary constituent of the proportional counter fill gas. This feature complicates the response of the proportional counters for energies above the absorption edge, because the resulting K X-ray, which is 2.97 keV for argon, may escape the detector. A corresponding escape peak will then appear in the spectrum that lies below the full-energy peak by an amount equal to this characteristic energy. This can be seen in Figure 2, which is the response of an unfiltered gas proportional counter to an Fe-55 source which emits the Mn K-alpha and K-beta lines at 5.899 and 6.490 keV, respectively. The fit to the measured pulse height spectrum (solid line) requires four peaks (dashed lines); one for the K-alpha line, one for the K-beta line and one for each of the two escape lines. The full energy peak for the K-alpha line is seen in channel 143.8. The corresponding escape peak is in channel 67.1. From the energy calibration provided in the table in the upper left-hand corner of Figure 2, this implies an energy difference of 2.97 keV, as predicted.

The measured absolute efficiency of a MESSENGER gas proportional counter at 5.9 keV is 0.83 ± 0.005 . This result was obtained by placing an Fe-55 source of known strength, on axis and at a fixed

FSCM NO. 88898	SIZE A	DRAWING NO. 7388-9061	REV. A
SCALE	DO NOT SCALE PRINT		SHEET 6 of 13

distance from the detector. The error reflects statistical uncertainty, only. Systematic errors are probably less than ~1%. Including the effect of non-uniform charge collection results in an absolute efficiency of 80% at 5.9 keV, that is in good agreement with the measurement.

The energy resolution of gas proportional counters varies inversely as the square root of the energy,

$$\Gamma = 2.35 \left(\frac{W(F + b)}{E} \right)^{1/2},$$

where Γ is the full-width at half-maximum (FWHM) as a fraction of the X-ray energy, W is the energy required to create an ion pair, F is the Fano Factor, b is a parameter that characterizes the avalanche statistics, and E is the energy in keV. (See, for example, Knoll 1989). This equation represents the statistical limit for a gas proportional counter, which is the best response one can expect. For P-10 these parameters are, $W=0.026$ keV/ion pair, $F=0.17$, and $b=0.50$. The above equation then becomes:

$$\Gamma = 0.310E^{-1/2},$$

At 5.9 keV this would imply an energy resolution of 12.8% or 0.753 keV. The energy resolution at 5.9 keV for the detector as shown in Figure 2 is 0.829 keV, or about 14.0%, which is typical for all the proportional counters on MESSENGER. An increase of about 10% over the statistical limit is expected for these detectors due to electronic noise and non-uniformity of the anode wire. The performance goal for the gas proportional counters was 15% energy resolution or better at 5.9 keV.

The response of a proportional counter to six different X-ray lines is shown in Figure 3. The pulse height spectra were generated by using an alpha particle excitation source on targets of Mg (1.254-keV), Al (1.487-keV), Si (1.740-keV), S (2.307-keV), Ca (3.690-keV), and Ti (4.508-keV). The fractional energy resolution of each of these six X-ray lines, plus the 5.899-keV line from Fe-55 is plotted versus energy in Figure 4. The fitted line is a power-law function in energy with a slope of -0.522 and a constant of proportionality of 0.364.

GPC Live Time

X-ray spectra collected during solar flare emissions will provide the best data on the surface composition of Mercury. However, the higher count rates that may be observed in the GPC during these times will result in both hardware and software event losses. In order to convert spectral peak areas to chemical compositions these losses must be quantified. The event loss rate for GPC2 is shown in Figure 5. At rates up to 1000 s^{-1} , losses are no more than ~4%. Even at rates greater than 5000 s^{-1} the total losses are only about 16%. All the GPCs were tested and displayed very similar results to those displayed in Figure 5. The design goal for the XRS was GPC lifetime greater than 90% for rates up to 1000 s^{-1} .

FSCM NO. 88898	SIZE A	DRAWING NO. 7388-9061	REV. A
SCALE	DO NOT SCALE PRINT		SHEET 7 of 13

GPC Filter Thickness

Below 2 keV, the X-ray lines of interest for geochemical purposes are Mg (1.254 keV), Al (1.487 keV), and Si (1.740 keV). Analysis of these three X-ray lines is complicated by the fact that they cannot be separately resolved by the proportional counters. The energy resolution of the proportional counters at these energies is nearly 30%, far too great to observe any separation of these lines. This is the reason for including the Mg and Al filters. The sharp K- edges of these two filters shown in Figure 1 preferentially allow different amounts of the three X-ray lines to be detected by the Mg- and Al-filtered detectors. The response of these two detectors and of the unfiltered detector are identical, except for these filters. Combining the spectral measurements from the two filtered detectors with that of the unfiltered detector makes the extraction of peak areas possible.

The thickness of the filters was determined by irradiating Mg and Ca target material with an Fe-55 source. The resulting lines at 1.254 and 3.690 keV, respectively, were detected by a GPC, with no filter, then a Mg filter, and finally an Al filter. Other than the addition of the filters, the geometry was unchanged during the measurements. Measuring the change in peak areas with and without filters determined filter thickness. The following results were obtained:

$$\text{Mg line Mg-filter/No-filter} = 0.553 \pm 0.009 = \exp(-504 \cdot 1.74 \cdot d) \Rightarrow d = (6.76 \pm 0.18) \cdot 10^{-4} \text{ cm}$$

$$\text{Ca line Mg-filter/No-filter} = 0.710 \pm 0.031 = \exp(-373 \cdot 1.74 \cdot d) \Rightarrow d = (5.28 \pm 0.68) \cdot 10^{-4} \text{ cm}$$

$$\text{Mg line Al-filter/No-filter} = 0.304 \pm 0.007 = \exp(-648 \cdot 2.70 \cdot d) \Rightarrow d = (6.81 \pm 0.13) \cdot 10^{-4} \text{ cm}$$

$$\text{Ca line Al-filter/No-filter} = 0.448 \pm 0.024 = \exp(-450 \cdot 2.70 \cdot d) \Rightarrow d = (6.61 \pm 0.45) \cdot 10^{-4} \text{ cm}$$

The modeled efficiencies in Figure 1 used filter thicknesses of 6.7 microns for both filters.

Proton Charging Test

On the NEAR XRS instrument, we observed charging in the insulator that is used to support the center anode of the GPC when it is exposed to energetic ions which resulted in a temporary degradation of the energy resolution (Floyd et al. 1999, Starr et al. 2000). It was later determined in a laboratory set-up that the charging was due to inadequate grounding of the insulator support. Hence, we have improved on the MESSENGER XRS GPC design by placing the insulator material between two fixed voltages. To verify the design, we tested a flight-like test counter with a radioactive source to charge up the insulator with ionizing particles. The test counter was irradiated for 1.5 hrs with a high counting rate (~10k cps) and no shift of the Fe-55 peak centroid or degradation of the energy resolution was observed. (Metorex performed test in September 2001).

Collimator Field-of-View

A collimated Fe-55 source was used to measure the response of XRS GPC over the entire field-of-view (FOV) of the instrument. We varied the incident angle from -7° to $+7^\circ$ relative to normal of the detector surface in two axes. The results are shown in Figures 6 and 7. During calibration the axes of rotation of the source were not aligned with the detector surface; an offset is required to transform the measured angle to true angle relative to the detector. In both figures, the dashed lines represent the measured data, the red curves represent the angle of rotation after the transformation, and the black curves represent the

FSCM NO. 88898	SIZE A	DRAWING NO. 7388-9061	REV. A
SCALE	DO NOT SCALE PRINT		SHEET 8 of 13

Gaussian fits. The FWHMs of the detector response with the collimator in place are $6.38 \pm 0.06^\circ$, and $5.70 \pm 0.05^\circ$ in the two dimensions. The corresponding full-widths at tenth-maximum (FWTM) are $11.68 \pm 0.12^\circ$ and $10.43 \pm 0.09^\circ$, respectively. (File FM GPC Collimator Calibrati.xls contains the report and measured data).

Background Rejection

The XRS gas proportional counters are relatively large in size, hence they are subject to a large number of background events from cosmic-ray and gamma-ray interactions in space. In order to address both types of background, the XRS employs two separate techniques to minimize the background: 1) Veto wires; 2) Pulse shape analysis.

Veto rejection

Twelve veto wires are placed around each circular shaped GPC covering 280° (except for the 80° of the opening window) and the entire length of the counter. There is no coverage at the ends of the counter. When ionizing particles or photons enter the counter active volume near one of the veto wires, they produce a “veto” event. If simultaneously (within ~ 10 microsecond coincidence window) there is also a signal in the center anode, the event will be vetoed and will not be registered as valid event. Monte Carlo simulations were performed to evaluate the coverage of the veto wires. Given an isotropically distributed background source, the veto wires will geometrically cover 82.93% of the full sky (4π). It is difficult to produce an isotropic background distribution while on ground during pre-flight calibration. Hence, we use the sea-level $\cos^2\theta$ muon distribution to serve as our background source to calibrate the veto efficiency. Figure 8 shows the background spectra we collected for 70 hours with both veto enabled and disabled. The efficiency is calculated to be 60%, while simulations show the veto wires will cover 70.5% geometrically for a $\cos^2\theta$ distribution. The discrepancy can be resolved since the veto wires will have approximately the same efficiency as the center anode ($\sim 85\%$) for gamma ray detection. Hence $70.5\% * 85\% = 60\%$ is consistent with the simulation results. The anticipated result in flight would then be $83\% * 85\% = 70.6\%$. (File: FM02 Background Rejection.xls; FM MXU Veto Rejection.xls)

Pulse shape discrimination

The veto wires provide an effective means to eliminate background for events that enter the counter in a region near a veto wire. However, the veto wires provide no protection when the cosmic rays enter the detector through the opening window or either end of the detector where there is no veto wire coverage. Fortunately, the interactions of these ions inside the detector are different than nominal X-ray events. Specifically, the rise time of the signal corresponding to ions is much slower than the signal corresponding to an X-ray. This is because most of the ions interact with the gas immediately after they enter the active volume of the gas counter, hence the generated electron clouds will have a longer transit to the center anode than the photon generated cloud that is closer to the center anode. In Figures 9 and 10, we show the rise time spectrum of valid events as a function of energy for both foreground (^{55}Fe at 5.89 keV) and background events (muons), respectively. (File: FM MXU Veto Rejection.xls; Rise time Rejection for Mg vs. Background.xls).

FSCM NO. 88898	SIZE A	DRAWING NO. 7388-9061	REV. A
SCALE	DO NOT SCALE PRINT		SHEET 9 of 13

Figure 11 shows a more detailed plot of the rise time as a function of acceptance percentage for three different energies at about the magnesium $K\alpha$ peak (1.25 keV). A threshold can be set to discriminate background events from valid X-ray events as a function of energy. The threshold is then determined by a line, with a zero-energy intercept and a slope. For each counter, both the slope and intercept can be adjusted separately by ground command. The slope of the line can be commanded between 0 and 1.6 ns per keV, and is nominally set to 0.8 ns per keV (8 ns difference over the full energy range). The zero-energy intercept can be commanded from 200 to 455 ns, with the default currently set to 350 ns. The settings have a minimum criterion of rejecting more than 75% of background events while accepting greater than 85% of the foreground. Settings can and will be verified for effectiveness during cruise operations. This will be accomplished during background measurements and during observations of CAS-A. This result does not meet the design goal of rejecting more than 90% of the background while accepting greater than 95% of the signal. Nevertheless, the impact on the science requirements is not great. The reduction in sensitivity as given in Table 5 of Solomon *et al.* (2001) still allows the XRS to meet its science goals.

Si-PIN SOLAR MONITOR

Solar Monitor Response and Efficiency

The MESSENGER solar monitor is a solid state Si-PIN diode. It is 500 microns thick with a 76 micron thick Be window and a 200-nm dead layer. The response of the detector was modeled using the Monte Carlo N-Particle eXtended (MCNPX) code and the result is shown in Figure 12 (Waters et al. 1999). The impact of the Be window on the efficiency at low energies is evident. The efficiency of the solar monitor at 5.9 keV was measured as described above for the gas proportional counters. The result was 0.982 ± 0.0007 , which is in good agreement with the calculated value of 0.96. The error reflects the statistical uncertainties, only. Systematic errors due to uncertainties in the source to detector distance are ~2%.

Figure 13 is a pulse height spectrum of the Si-PIN with an Fe-55 source in the field of view. The K-alpha and K-beta lines merge, but are separated by the fit. The FWHM of the K-alpha line (5.9 keV) is 635 eV or 10.8%. This result is greater than the design goal of 8.5%, but satisfies the scientific requirements of the XRS since it does not impact the ability to interpret the measured solar spectra and normalize the GPC measurements. Unlike the proportional counters, the energy resolution of the Si-PIN is determined primarily by the pre-amplifier noise and will not vary significantly over the energy region of interest.

Solar Monitor Live Time

The solar monitor will experience very high count rates during solar flares and must be capable of operating at rates in excess of 50000 s^{-1} . Figure 14 displays the solar monitor total event loss rate. For a maximum input rate of 42100 s^{-1} , the loss rate for the solar monitor was 56%. The design goal for this portion of the XRS electronics was live time greater than 50% for count rates up to 50000 s^{-1} . This reduced lifetime at high rates, is not an issue, and will not impact our science requirements. Spectra will still be collected with good statistics at the very highest rates, live time is measured accurately and most importantly, the shape of the spectrum is not distorted.

FSCM NO. 88898	SIZE A	DRAWING NO. 7388-9061	REV. A
SCALE	DO NOT SCALE PRINT		SHEET 10 of 13

Collimator Field-of-View

A collimated Fe-55 source was also used to measure the FOV of the Si-PIN solar monitor. Figure 15 shows the measured angular response of the SAX detector from -30° to $+30^\circ$ relative to normal. The measurement confirms the 42° full angle cone of the XRS opening, and the FWHM of the FOV is $52 \pm 2^\circ$. The slight asymmetry in the data may be due to a slight misalignment of the source relative to the center of the detector.

FSCM NO. 88898	SIZE A	DRAWING NO. 7388-9061	REV. A
SCALE	DO NOT SCALE PRINT	SHEET 11 of 13	

REFERENCES

Adler, I., J. I. Trombka, J. Gerard, P. Lowman, R. Schamadebeck, H. Blodgett, E. Eller, L. Yin, R. Lamothe, P. Gorenstein, and P. Bjorkholm 1972a. Apollo 15 geochemical X-ray fluorescence experiment: Preliminary report, *Science*, **175**, 436-440.

Adler, I., J. Gerard, J. I. Trombka, R. Schamadebeck, P. Lowman, H. Blodgett, L. Yin, E. Eller, and R. Lamothe 1972b. The Apollo 15 X-ray fluorescence experiment, *Proc. Lunar Sci Conf. 3rd*, 2157-2178.

Adler, I., J. I. Trombka, J. Gerard, P. Lowman, R. Schamadebeck, H. Blodgett, E. Eller, L. Yin, R. Lamothe, G. Osswald, P. Gorenstein, P. Bjorkholm, H. Gursky, and B. Harris 1972c. Apollo 16 geochemical X-ray fluorescence experiment: Preliminary report, *Science*, **177**, 256-259.

Floyd, S. R., J. I. Trombka, H. W. Leidecker, P. E. Clark, R. Starr, J. O. Goldsten, and D. R. Roth 1999. Radiation Effects on the Proportional Counter X-Ray Detectors on Board the NEAR Spacecraft, *Nucl. Inst. and Meth. In Phys. Res. A* **422**, (1999) 577-581.

Goldsten, J. O., R. L. McNutt, Jr., R. E. Gold, S. A. Gary, E. Fiore, S. E. Schneider, J. R. Hayes, J. I. Trombka, S. R. Floyd, W. V. Boynton, S. Bailey, J. Brückner, S. W. Squyres, L. G. Evans, P. E. Clark and R. Starr 1997. The X-Ray/Gamma-Ray Spectrometer on the Near Earth Asteroid Rendezvous Mission, *Space Sci. Rev.* **82**, 169-216.

Knoll, G. F. 1989. *Radiation Detection and Measurement*, John Wiley & Sons, New York, Chapter 6.

Starr, R., P. E. Clark, L. G. Evans, S. R. Floyd, T. P. McClanahan, J. I. Trombka, J. O. Goldsten, R. H. Maurer, R. L. McNutt, Jr., and D. R. Roth 1999. Radiation Effects in the Si-PIN Detector on the Near Earth Asteroid Rendezvous Mission, *Nucl. Inst. and Meth. In Phys. Res. A* **428**, 209-215.

Starr, R., P. E. Clark, M. E. Murphy, S. R. Floyd, T. P. McClanahan, L. R. Nittler, J. I. Trombka, L. G. Evans, W. V. Boynton, S. H. Bailey, J. Bhangoo, I. Mikheeva, J. Brückner, S. W. Squyres, E. M. McCartney, J. O. Goldsten, and R. L. McNutt, Jr. 2000. Instrument Calibrations and Data Analysis Procedures for the NEAR X-Ray Spectrometer *Icarus* **147**, 498-519.

Solomon, S. C., McNutt, R. L., Gold, R. E., Acuña, M. H., Baker, D. N., Boynton, W. V., Chapman, C. R., Cheng, A. F., Gloeckler, G., Head, J. W., III, Krimigis, S. M., McClintock, W. E., Murchie, S. L., Peale, S. J., Phillips, R. J., Robinson, M. S., Slavin, J. A., Smith, D. E., Strom, R. G., Trombka, J. I., Zuber, M. T. 2001. The MESSENGER mission to Mercury: scientific objectives and implementation *Planetary and Space Science*, **49**, 1445-1465.

Waters, L. S., Ed., MCNPX User's Guide (document LA-UR-99-6058) (Los Alamos National Laboratory, Los Alamos, NM, 1999).

Yin, L. I, J. I. Trombka, I. Adler and M. Bielefeld 1993, X-ray Remote Sensing Techniques for Geochemical Analysis of Planetary Surfaces, In *Remote Geochemical Analysis: Elemental and*

FSCM NO. 88898	SIZE A	DRAWING NO. 7388-9061	REV. A
SCALE	DO NOT SCALE PRINT		SHEET 12 of 13

Mineralogical Composition, pp. 199-212, (C. Pieters and P. Englert eds.), Cambridge University Press.

FSCM NO. 88898	SIZE A	DRAWING NO. 7388-9061	REV. A
SCALE	DO NOT SCALE PRINT		SHEET 13 of 13